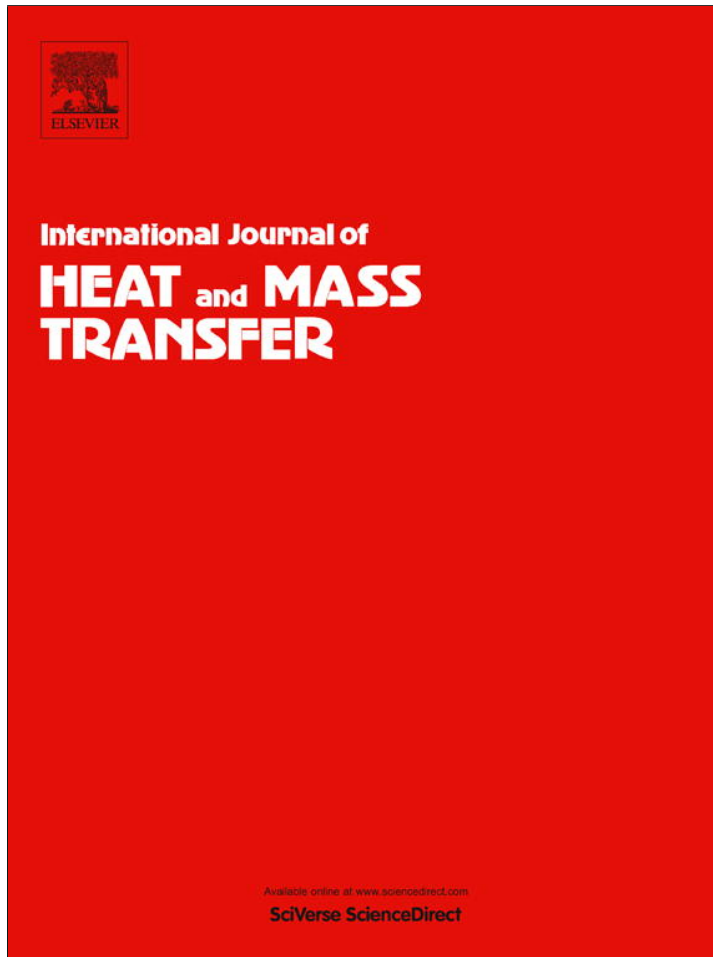


Provided for non-commercial research and education use.
Not for reproduction, distribution or commercial use.



This article appeared in a journal published by Elsevier. The attached copy is furnished to the author for internal non-commercial research and education use, including for instruction at the authors institution and sharing with colleagues.

Other uses, including reproduction and distribution, or selling or licensing copies, or posting to personal, institutional or third party websites are prohibited.

In most cases authors are permitted to post their version of the article (e.g. in Word or Tex form) to their personal website or institutional repository. Authors requiring further information regarding Elsevier's archiving and manuscript policies are encouraged to visit:

<http://www.elsevier.com/authorsrights>



Laser processing by using fluidic laser beam shaper

Hong Duc Doan ^{*}, Iwatani Naoki, Fushinobu Kazuyoshi

Tokyo Institute of Technology, Box 16-3 Meguro-ku, Tokyo 152-8550, Japan



ARTICLE INFO

Article history:

Received 30 December 2012

Received in revised form 17 April 2013

Accepted 17 April 2013

Keywords:

Laser drilling
Fluidic laser beam shaper
Beam profile
Flat-top beam
Annular beam

ABSTRACT

Laser beam shaping techniques are important to optimize a large number of laser material processing applications and laser-material interaction studies. The authors have developed a novel Fluidic Laser Beam Shaper (FLBS) with merits such as flexibility, versatility and low cost. This work presents a fundamentally new approach for laser beam shaping by using FLBS. A Gaussian beam profile is transformed to a flat top beam and an annular beam profile in the focal plane. The shaped laser beam is used for laser drilling to investigate the influence of the laser intensity profile in laser processing. The paper concludes with suggestions for future research and potential applications for further the work.

© 2013 Elsevier Ltd. All rights reserved.

1. Introduction

Laser machining (drilling, cutting, carving, etc.) has been recognized to be a useful and competitive method of material processing especially for hard materials, curved surfaces and hard to access places. The most frequently employed lasers for material processing are CO₂, Nd:YAG and excimer lasers. These lasers have provided the microelectronics and automotive sector in particular, with an effective tool for producing high quality micro-holes. However, in the case of long pulsed lasers, it is well known that laser micromachining can be quite complicated by collateral thermal effect such as melt, recast and heat affect zone (HAZ) [1–3]. Important factors in the laser processing of materials include energy, fluence, spot size, wavelength, polarization, pulse duration and repetition rate [1–3]. The role of these parameters has been widely studied, both experimentally and theoretically [1–3]. However, most of the previous work has been done with Gaussian beam, which has a Gaussian transverse intensity profile with the spot area limited by a beam diameter ($FW1/e^2M$) contains only 86.5% of the laser beam power and intensity at the boundary is only 13.5% of the peak intensity. It means that, the energy in wings is lost or can even cause damage of surrounding material as well as a high-intensity central peak. Therefore, non-Gaussian beam should be able to give us more choice to determine the optimum processing conditions.

Although, non-conventional beam shapes have an advantage in which they can be explicitly designed to meet the requirements of a given material configuration or application, studies on the influence of the laser intensity profile in laser processing is still limited [4–8]. One reason is that it is difficult to control the beam shaping process. Current beam shaping technique require complex designs of optical systems which are very expensive. Most previous works are more concentrated in laser shaping techniques and still lack detailed discussion of thermal effect on processed product.

The authors have developed a novel FLBS with some merits as flexible, versatile and low cost [9,10]. This work presents a fundamentally new fabrication approach for laser beam shaping by using FLBS with long pulse (microsecond pulse). The Gaussian beam was transformed to a flat-top and annular beam. The shaped laser beam was applied for laser drilling to investigate the influence of the laser intensity profile in laser hole qualities such as: geometric features and HAZ.

2. Shaping of the processing laser beam

Fig. 1 shows the schematic of the experimental set up for shaping the Gaussian beam by using a single beam thermal lens system. Detail of laser beam shaping process was discussed in previous work [9]. A fiber laser (JenLas® fiber) is used as pump/processing laser ($P_{max} = 100$ W, $\lambda = 1070$ nm, $\Phi = 5.0$ mm, TEM00). Laser is operated at pulse mode with pulse width of 30 μ s and repetition rate of 10 kHz. The cuvette is a three-layer structure with a sheet copper sandwiched between two pieces of fused silica. The thick-

* Corresponding author. Tel./fax: +81 3 5734 2500.

E-mail address: doan.d.aa@m.titech.ac.jp (H. Duc Doan).

Nomenclature

D	normalization hole diameter, mm	D_h	hole diameter, mm
D_b	beam diameter, mm	ΔD	normalization discoloration diameter, mm
D_c	discoloration diameter, mm		

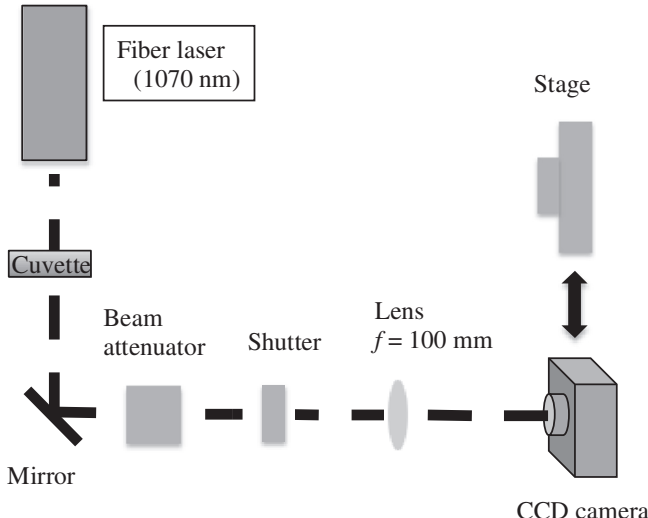


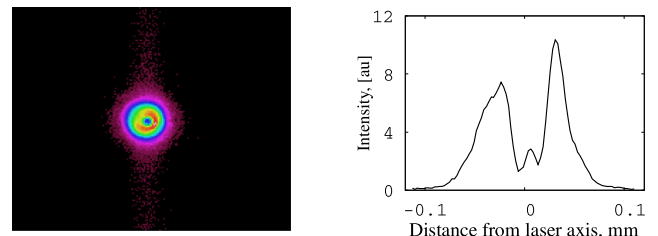
Fig. 1. Schematic illustration of the experimental set up for shaping the Gaussian beam and using it for laser processing.

ness of the fused silica is 1 mm. The sheet copper has annular shape. The liquid that is contained inside the annular hole has the same height with the sheet copper thickness. By changing the thickness of the sheet copper, the liquid height can be changed. The ethanol solution dissolved dye (Sunset-yellow) was filled in the cuvette. In this experiment, the thickness of liquid is 0.3 mm, and the measure absorption coefficient of liquid is 0.05 cm^{-1} . The measurements of beam profile are made with a CCD camera (BeamStar FX 50) using a $4\times$ beam expander with the spatial resolution of $2.5 \mu\text{m} \times 2.5 \mu\text{m}$.

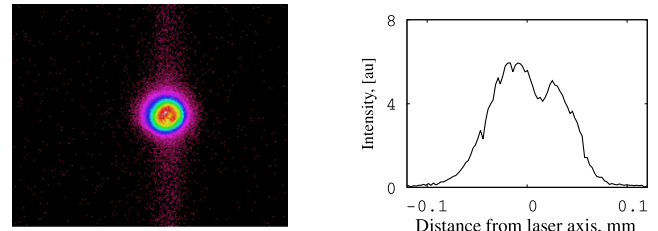
The fiber laser irradiates the cuvette to form a FLBS. The pump power can be changed by current control. After passing through the cuvette, the power of laser is adjusted again by an external attenuator including a variable beam splitter and a correction plate. Then, the processing laser is directed towards the CCD camera located on the 2D stage position after focusing by a 100 mm focal length convex quartz lens. Details of the experimental parameters for beam shaping process are shown in Table 1.

Table 1
Experimental conditions.

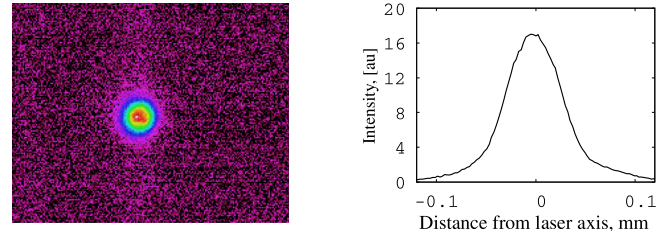
Wave length, nm	1070 ± 10
Pulse width, μs	30
Repetition rate, kHz	10
Pump power, W	1–100
Processing power, W	9
Focal length, mm	100
M^2 value	<1.1
Beam waist, mm	4.5–5.5
Absorption coefficient, cm^{-1}	0.05
Distance from cuvette to lens, mm	435



(a) Annular beam (pump power: 27 W)



(b) Flat top beam (pump power: 12.6 W)



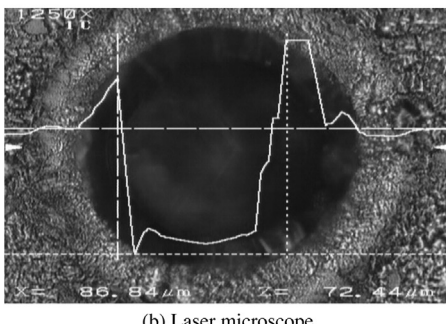
(c) Gaussian beam

Fig. 2. Transverse beam intensity profile and its cross-section captured by the CCD camera at the difference power of the pump laser.

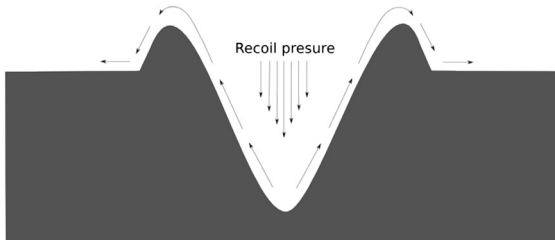
As shown in the previous work, the intensity profile of the processing laser can be controlled by adjusting some parameters in thermal lens effect such as: the pump power, absorption coefficient and the propagation distance [9]. First, the pump power is fixed at 12.6 W and the CCD camera is scanned along the propagation axis to find the location of the flat top beam. Then, the CCD camera is fixed, and the pump power is increased to 27 W to generate an annular beam. Finally, the cuvette is replaced, and the CCD camera is scanned along propagation axis to find the location again in which Gaussian beam has a same beam waist as the flat top beam and the annular beam. Fig. 2 shows transverse beam intensity profile and its cross-section captured by the CCD camera at the different power of the pump laser. The left figure shows the beam shape and the right figure shows the intensity distribution. In the right figure, the vertical and horizontal axes show intensity and distance from the laser axis respectively. With increasing pump power, the laser beam profile changes from Gaussian to flat-top and an annular beam profile respectively.



(a) SEM picture



(b) Laser microscope



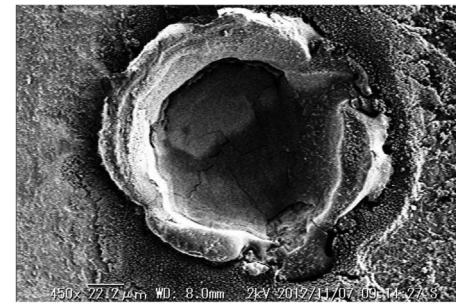
(c) Schematic diagram depicting recoil pressure force acting on the molten pool

Fig. 3. Picture of a hole drilled by a Gaussian beam after 1 s.

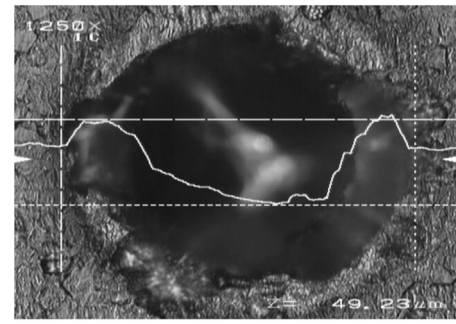
3. Laser processing with shaped beam

After confirming the intensity profile of the processing laser, the CCD camera and ND filter is replaced by a metal sample for the drilling process. A pure titanium bulk sample (purity: 99.999%, size: 10 mm × 10 mm × 0.1 mm) was used as the sample in this experiment. The quality of processing was evaluated with an optical microscope (KEYENCE VF7500) and a scanning electron microscope (KEYENCE VE8800). During the drilling process, the power of the processing laser was adjusted to 9 W for the Gaussian, flat-top and annular beam. Details of the experimental parameters for the drilling process is shown in Table 1.

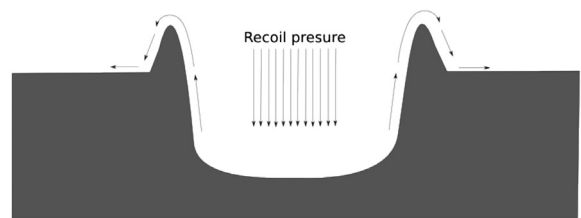
Geometric features of holes drilled with different beam shapes are shown in Figs. 3–8. In these figures, (a) is a SEM image, (b) is a laser microscope image (solid white line shows hole's cross-section profile), (c) is schematic diagram depicting recoil pressure force acting on the molten pool and the melt flow. As shown in Fig. 3(a) and (b), the hole has a Gaussian-like shape with high recast layer (about 40 μm, 55% of hole depth) on the rim. During the laser drilling process, the surface temperature of the sample rises and the materials goes to a molten state, leading to vaporization. This vapor generates a recoil pressure on the melt surface with a force much greater than the surface tension of the melt [11,12]. Due to the Gaussian intensity distribution of the laser beam, there exists a pressure gradient in the radial direction of the beam due to the decreasing laser intensity. At the same time, due to the presence of the huge temperature gradient, which causes the strong



(a) SEM picture



(b) Laser microscope



(c) Schematic diagram depicting recoil pressure force acting on the molten pool

Fig. 4. Picture of a hole drilled by a flat-top beam after 1 s.

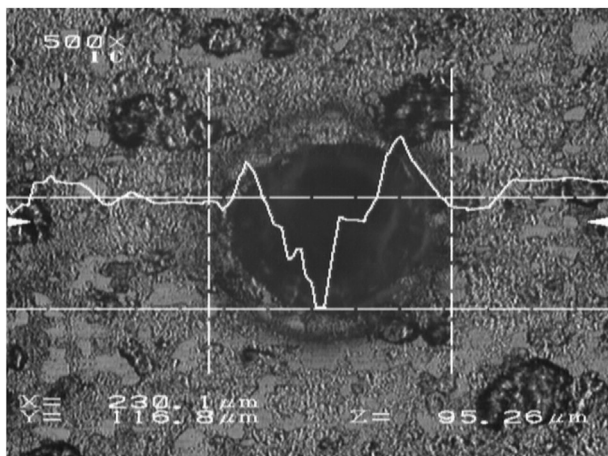
Marangoni shear stress, the molten surface fluid at the melt pool center is driven along the wall of the crater and is expelled from the entrance of the drilled hole as shown in Fig. 3(c). It is worth noting that during the laser pulse interaction with the sample, the recoil pressure is the dominant driving force.

Figs. 4 and 5 show the geometric features of a hole drilled with a flat top beam after 1 s and 5 s, respectively. As shown in Fig. 4(a) and (b), hole drilled after 1 s has a flat bottom with lower recast layer (about 15.7 μm, 47% of hole depth) than that of the hole drilled with Gaussian beam. As shown in Fig. 5(a) and (b), hole drilled after 5 s has a Gaussian-like shape with high recast layer (about 30 μm, 25% of hole depth) on the rim. Detailed mechanism of the change in the hole shape with irradiation time occurs as follows. When the irradiation time is short, the temperature distribution on the sample surface is dominated by the beam profile. Therefore, the temperature distribution and the recoil pressure distribution is almost flat at the center of the melt pool as shown in Fig. 4(c). As a consequence, the bottom of the hole is more flatter than that of hole drilled with the Gaussian beam. However, with increasing irradiation time, the temperature field reaches the quasi-steady state with the parabolic-like temperature distribution due to heat conduction [13]. Therefore, the temperature distribution and the recoil pressure distribution tend to approach the same distribution with which is caused by Gaussian beam. As a consequence, the hole drilled after 5 s has a Gaussian-like shape.

Figs. 6 and 7 show geometric features of a hole drilled with an annular beam after 1 s and 5 s, respectively. As shown in Fig. 6(a)



(a) SEM picture



(b) Laser microscope

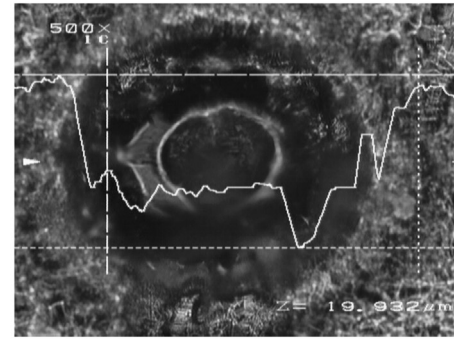
Fig. 5. Picture of a hole drilled by a flat-top beam after 5 s.

and (b), hole drilled after 1 s has a doughnut shape with a deepest area in the circular zone. In the hole center, the rim part is slightly higher than the center part. As shown in Fig. 7(a) and (b), hole drilled after 5 s has a flat bottom like that drilled with a flat top beam after 1 s. Detailed mechanism of the change in the hole shape with irradiation time occurs as follows. When the irradiation time is short, the surface temperature distribution on the sample is dominated by the beam profile. Corresponding to the intensity distribution which concentrates in a ring band area, the melt pool is initiated at the ring band region. As shown in Fig. 6(c), the recoil pressure distribution concentrates in the ring band and molten fluid is driven away from the band region, which exists both inward and outward in the radial direction. The inward flow drives the molten fluid upward, which causes the rim of the central part to be slightly higher than the center.

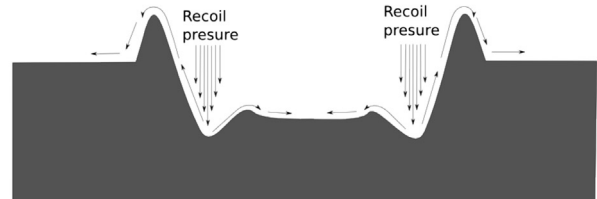
On the other hand, the molten fluid transports the enthalpy from the ring to center and melts the material in the center region. During this process, the enthalpy is transported more and more to center to make the temperature in center region increase and temperature in ring region decrease. After a certain time, the temperature in the center region becomes higher than in ring region. As a consequence, the molten fluid in center region changes its direction from inward to outward as shown in Fig. 7(c). Subsequently, the molten fluid, which is pushed away by the outward flow in the ring band region is compensated by the fluid from the central region to make the bottom of the hole become flat. Another reason



(a) SEM picture



(b) Laser microscope



(c) Schematic diagram depicting recoil pressure force acting on the molten pool

Fig. 6. Picture of a hole drilled by an annular beam after 1 s.

is the contribution of heat conduction. As mentioned in [13], with increasing irradiation time, the temperature field reaches the quasi-steady state with the flat top temperature distribution due to heat conduction. This temperature field also tends to make the bottom of the hole become flat. To answer the interesting question why the same mechanism does not occur between the ring and the rim regions, this is because the center region has smaller area than the ring and rim regions, which tends to increase its temperature faster than the other region receiving the same amount of energy.

Fig. 8 shows a comparison in which the diameter and depth of the hole that has been processed by three types of the beam profiles. However, the diameter of the hole has been normalized by the Eq. (1) using the beam diameter. Data in this figure is the average value of five experimental data points; error bars show the maximum and minimum values.

$$D = \frac{D_h}{D_b} \quad (1)$$

Here, D is normalized diameter, D_h is hole diameter, D_b is beam diameter.

As shown in Fig. 8, as hole diameter increases, hole depth decreases in the order Gaussian beam, top-hat beam and annular beam. In other words, the aspect ratio of the hole decreases in the order of Gaussian beam, top-hat beam and annular beam.

Fig. 9 shows a laser microscope image of a hole drilled by a Gaussian beam after 1 s with a discoloration area around a rim of the

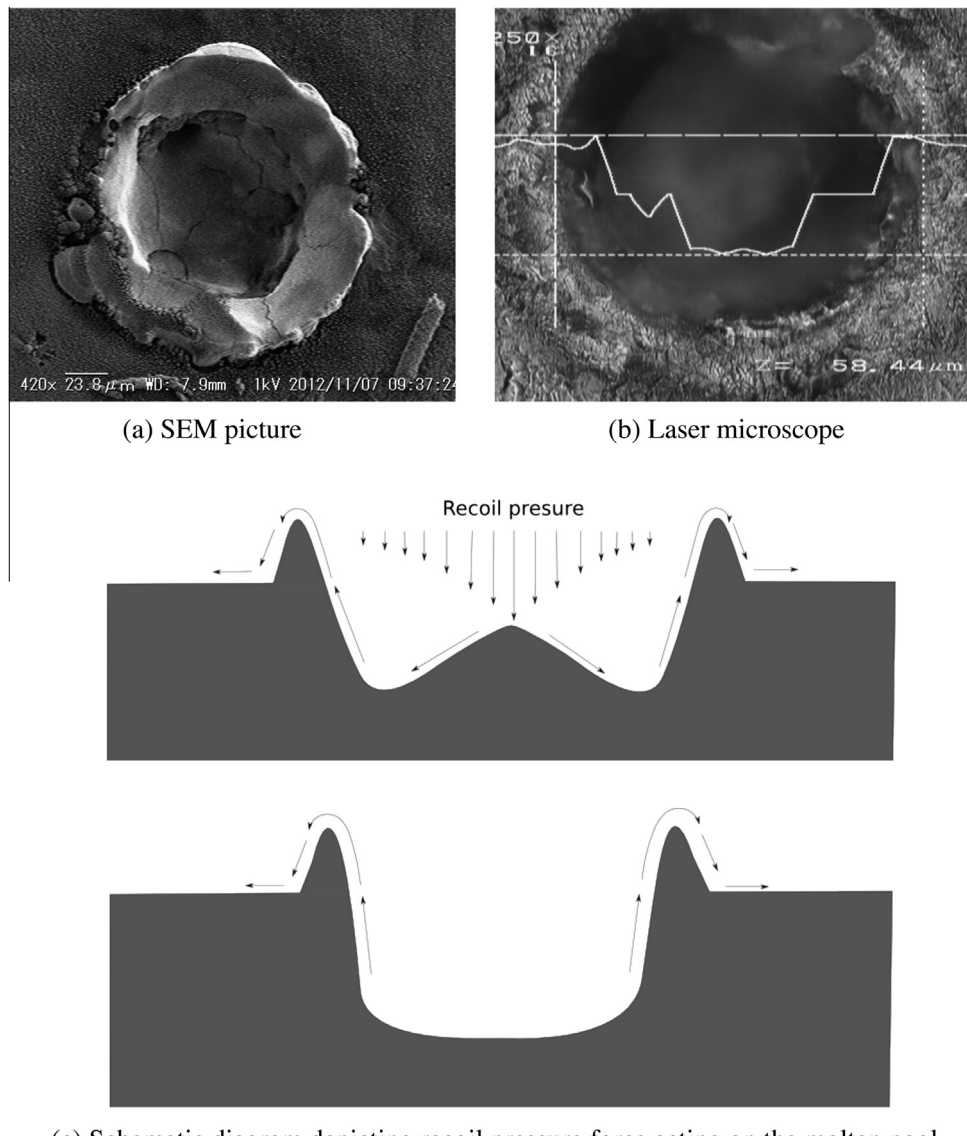


Fig. 7. Picture of a hole drilled by an annular beam after 5 s.

hole. This discoloration is observed when the white light is reflected from the top and bottom boundaries of the oxide film on the sample surface. During the drilling process, the samples were superficially melted by the laser beam leading to oxygen diffusion through the molten material and, thus, to the oxidation of titanium. Therefore, the discoloration area shows the heat affected zone in surface. Fig. 10 shows the diameter of the discoloration area around the hole that has been processed by three types of the beam profile. However, the diameter of the discoloration has been normalized by the Eq. (2) using the beam diameter and hole diameter. Data in this figure is the average value of five experimental data points, error bars show the maximum and minimum values.

$$\Delta D = \frac{D_c - D_h}{D_b} \quad (2)$$

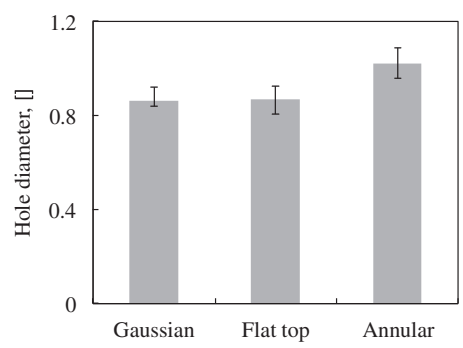
Here, ΔD is normalized diameter of the discolored area, D_c is the diameter of the discolored area.

As shown in Fig. 10, the normalized diameter of the discolored area decreases in the order of Gaussian beam, top-hat beam and

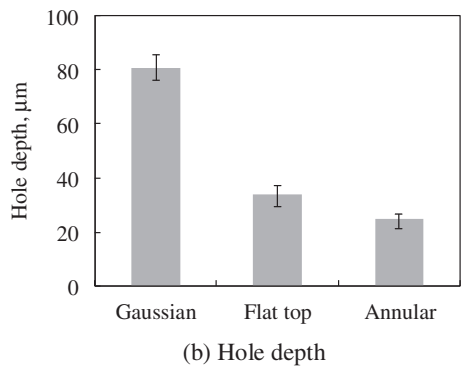
annular beam. This means that, HAZ decreases in the order of Gaussian beam, top-hat beam and annular beam. During laser drilling process, HAZ is dominant by mechanisms of heat dissipation from irradiation area, which include heat conduction and heat convection. If the heat conduction is the dominant, HAZ should increase in the order Gaussian beam, top-hat beam and annular beam [13]. Therefore, HAZ is dominated by heat convection. As a consequence, a hole drilled by a Gaussian beam with the thickest recast layer has the largest HAZ.

4. Conclusion

In this work, FLBS is used to shape the Gaussian beam to a flat top beam and annular beam. The shaped laser beam was applied for laser drilling. When the laser irradiation time is short, the hole is formed with the shape similar to the laser beam profile. However, when the laser irradiation time is long, the hole which forms tends to have a shape similar to that which is drilled by a Gaussian beam. The diameter of drilled hole increases, its depth decreases and its aspect ratio decreases in the order of Gaussian beam, top-



(a) Hole diameter



(b) Hole depth

Fig. 8. Comparison of depth and diameter of holes drilled by three types of laser beam profile.

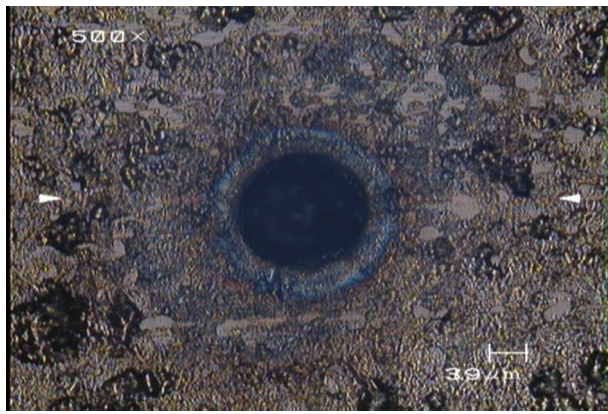


Fig. 9. Picture of a hole drilled by Gaussian beam with discoloration area.

hat beam and annular beam. The HAZ decreases in the order of Gaussian beam, top-hat beam and annular beam.

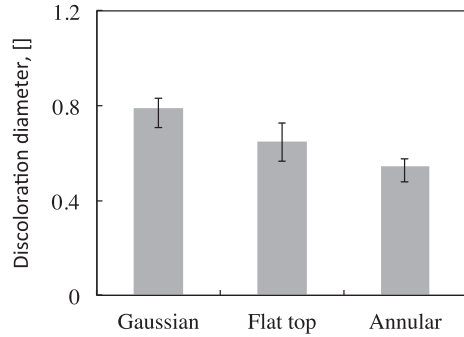


Fig. 10. Comparison of discoloration diameter of holes drilled by three types of laser beam profile.

Acknowledgement

Part of this work has been supported by the Grant-in-Aid for JSPS Fellows from MEXT/JSPS. The authors also would like to acknowledge the Center for Monotsukuri in Tokyo Institute of Technology for use of their SEM facility.

References

- [1] W.M. Steen (Ed.), *Laser Materials Processing*, Springer, London, 1991.
- [2] S.P.H. Narendra, B. Dahotre (Eds.), *Laser Fabrication and Machining of Materials*, Springer, New York, NY, 2008.
- [3] E. Kannatey-Asibu (Ed.), *Principles of Laser Materials Processing*, John Wiley & Sons, Inc., Hoboken, NJ, 2009.
- [4] G. Raciuikaitis, E. Stankevicius, P. Gecys, M. Gedvilas, C. Bischoff, E. Jager, U. Umhofer, F. Volklein, Laser processing by using diffractive optical laser beam shaping technique, *JLMN J. Laser Micro/Nanoeng.* 6 (1) (2011) 37–43.
- [5] D.M. Karnakis, J. Fieret, P.T. Rumsby, M.C. Gower, Microhole drilling using reshaped pulsed Gaussian laser beams, in: Proceedings of SPIE, vol. 4443, 2001.
- [6] L. Han, F.W. Liou, Numerical investigation of the influence of laser beam mode on melt pool, *Int. J. Heat Mass Transfer* 47 (2004) 4385–4402.
- [7] S. Safdar, L. Li, M.A. Sheikh, L. Zhu, Finite element simulation of laser tube bending: effect of scanning schemes on bending angle, distortions and stress distribution, *Opt. Laser Technol.* 39 (2007) 1101.
- [8] Cyril Hnatovsky, Vladlen G. Shvedov, Natalia Shostka, Andrei V. Rode, Wieslaw Krolikowski, Polarization-dependent ablation of silicon using tightly focused femtosecond laser vortex pulses, *Optics Lett.* 37 (2) (2012) 226–228.
- [9] D.H. Doan, Y. Akamine, K. Fushinobu, Fluidic laser beam shaper by using thermal lens effect, *Int. J. Heat Mass Transfer* 55 (2012) 2807–2812.
- [10] D.H. Doan, K. Fushinobu, Fluidic optical devices based on thermal lens effect, *Optical Devices in Communication and Computation*, INTECH, 2012. Chapter 9.
- [11] V.V. Semak, G.A. Knorovsky, D.O. MacCallum, R.A. Roach, Effect of surface tension on melt pool dynamics during laser pulse interaction, *J. Phys. D Appl. Phys.* 39 (2006) 590.
- [12] A.K. Nath, D. Hansdah, S. Roy, A. Roy Choudhury, A study on laser drilling of thin steel sheet in air and underwater, *J. Appl. Phys.* 107 (2010) 123103.
- [13] M. Duocastella, C.B. Arnold, Bessel and annular beams for materials processing, *Laser Photonics Rev.* (2012) 1–15.